

Intuitive Shape Editing in Latent Space

Tim Elsner Moritz Ibing Victor Czech Julius Nehring-Wirxel Leif Kobbelt
Visual Computing Institute, RWTH Aachen University

Abstract

The use of autoencoders for shape generation and editing suffers from manipulations in latent space that may lead to unpredictable changes in the output shape. We present an autoencoder-based method that enables intuitive shape editing in latent space by disentangling latent sub-spaces to obtain control points on the surface and style variables that can be manipulated independently. The key idea is adding a Lipschitz-type constraint to the loss function, i.e. bounding the change of the output shape proportionally to the change in latent space, leading to interpretable latent space representations. The control points on the surface can then be freely moved around, allowing for intuitive shape editing directly in latent space.

We evaluate our method by comparing it to state-of-the-art data-driven shape editing methods. Besides shape manipulation, we demonstrate the expressiveness of our control points by leveraging them for unsupervised part segmentation.

1. Introduction

Creating new 3D shapes and editing existing ones is a key task in computer graphics. Having the ability to interactively design shapes is an ongoing part of research [8, 16, 30, 39]. In particular, designing different variations of an item from a collection of shapes can be cumbersome. These applications can benefit from tools that guide the user with learned semantic expertise, such as enforcing symmetry for airplane wings, or having chair legs attached to the seating area. Recent approaches in deep learning like Generative Adversarial Networks (GANs) [14] can be used to generate new examples of a given shape collection [27], but usually offer little intuitive manipulability [20, 21], or require complex regularisation techniques [6, 32] that can not be transferred to geometry easily.

Autoencoders [25] are an established way to learn efficient encodings without any supervision and provide a parametric representation of a given shape collection that is in principle manipulable. While a basic autoencoder, and even more so its derivatives [19, 23, 37], can be used

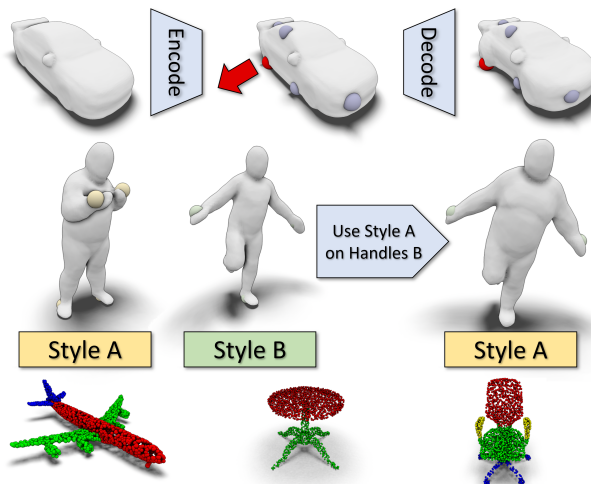


Figure 1. Proposed applications of our learned latent space (top to bottom; dots in the model show latent code of the handles): Shape editing performed on a car (red handle moved outwards), style transfer from one humanoid to another, results of part segmentation based on the learned semantics of the handles.

for shape editing, this process is not controllable or intuitively interpretable. Motivated by the observation that the most user-friendly forms of shape editing are built around controlling the surface through manipulating control points (*handle points*) on the shape directly [18], we propose an autoencoder that does not use some arbitrary, hard to interpret latent code, but uses a small number of interpretable 3D handle points instead. The handle points themselves represent the coarse structure of the shape. As surface details or regions unrelated to handle points are not properly represented by these. To compensate this, we introduce a style vector holding all information that is not fully determined by the handle points. We disentangle style information and handle information by enforcing any latent change to be proportional to the output change. As a result, tiny variations in the handle positions can not encode important shape information, leading to intuitively manipulable handle points. As we need consistent handle points across shapes for this, we also provide a simple technique to obtain

these for a shape collection.

Different options can be considered to represent geometry in an autoencoder: Explicit representations like point clouds can suffer from artifacts. For example, having the same chair with a wider backrest will either require more points (impossible for a pointcloud autoencoder with fixed output size) or to spread out the existing ones, resulting in inconsistent point density. Voxelisation requires large amounts of memory to work with reasonable resolutions. Generating and processing triangle meshes is complex and cumbersome, as convolutions are complicated to define and properties like 2-manifoldness are difficult to produce [11, 45]. Instead, we propose to use an implicit autoencoder, based upon the implicit decoder DeepSDF by Park *et al.* [34].

Contribution This paper introduces a new way of training autoencoders to exhibit an interpretable latent code consisting of manipulable handle points and an interchangeable style vector. This allows for interactive adaptive shape editing as shown in Fig. 1. The coarse structure of the shape can be controlled through the handles directly, while the style can be changed independently. To obtain proper disentanglement of handles and style and to assure a smooth transition when adjusting the handles, we introduce a regularisation technique that tethers change in the latent space representation to a respective change in the output. This means that small movements to the handles or the style cause small differences in the output, and that applying changes to the style and handles is independent of each other. We further introduce a technique allowing changes in one part of the shape to adaptively propagate to the rest, *e.g.* keeping the symmetries of an airplane’s wings when moving a handle on one of them. To demonstrate the semantic power now embedded in the handles, we show a simple part segmentation approach. We also compare to other shape editing approaches.

2. Related Work

To make our latent space editable, we rely on disentangling the latent space into a shape related handle part, and a style vector. We enforce a disentanglement in order to achieve interpretable shape deformations. Hence, our work is mostly related to approaches either applying shape deformations or disentangling the latent space representation of an input.

Disentanglement Disentangling an input into semantically different components is an ongoing part of research. Approaches like Beta-VAEs [19] offer such disentanglement, which can also be transferred to geometry [47]. This yields decomposition of the latent space in different attributes, but lacks interpretability. Aumentado-Armstrong

et al. [3] split the latent space into a part representing the intrinsic geometry of the shape and its extrinsic pose. However, their latent space is still not interpretable, while we explicitly describe the pose of our shape through handle positions. Methods like [48] or [33] disentangle shapes into a structure part represented by a part hierarchy and shape details encoded in latent vectors. However, their output geometries are only controllable through (unintuitive) latent manipulation.

Shape deformation There are many previous works that discuss how one shape can be deformed to match the geometry of a target shape as close as possible. By restricting the deformation space, the shape still keeps the topology and some details of the original shape, but the possible alignment is rather limited. The presented methods differ mostly in the way they represent the deformation space. Yumer *et al.* [50] compute control points in a grid and use those to describe transformations. The is then moved according to a blending of these points. Gadelha *et al.* [12] generate shapes handles that can be used for deformation, while Gao *et al.* [13] learn part-based deformations. Tan *et al.* [43] use a variational autoencoder to deform meshes. Other approaches deform from a source to a target shape by deforming a geometric proxy [17, 49] allow deformations from source to partial targets by learning grid-based deformations. Lui *et al.* [30] proposed grouping handles working with biharmonic coordinates together into metahandles that can be manipulated. The resulting disentangled handles smoothly edit the shape, but are not part of the shape space itself. Sung *et al.* [42] learn transfer deformations from one shape to another by parameterizing the deformations themselves through an autoencoder. In contrast, our approach does not transform a source shape, but instead the shape itself is parameterized in part by these handles. Atzmon *et al.* [2] on the other hand do not try to give an intuitive transformation operator, but restrict latent interpolation to adhere to deformation constraints. To ease disentanglement, some approaches like Yang *et al.* [48] utilize labeled input data. In contrast to the previous approaches, our work achieves proper editability *through* a regularisation that produces disentanglement. Our approach has the advantage of consistent control points over different shapes that lie on the object itself and can hence be manipulated intuitively.

3. Learning Adaptive Shape Editing

Learning to autoencode shapes from a collection in an interpretable, adaptive, and manipulable way is achieved through using the following network architecture (see Fig. 2):

The encoder is computing three distinct pieces: First, a set of 3d handles on the surface of the shape that are holding most of the coarse structural information. Second, a

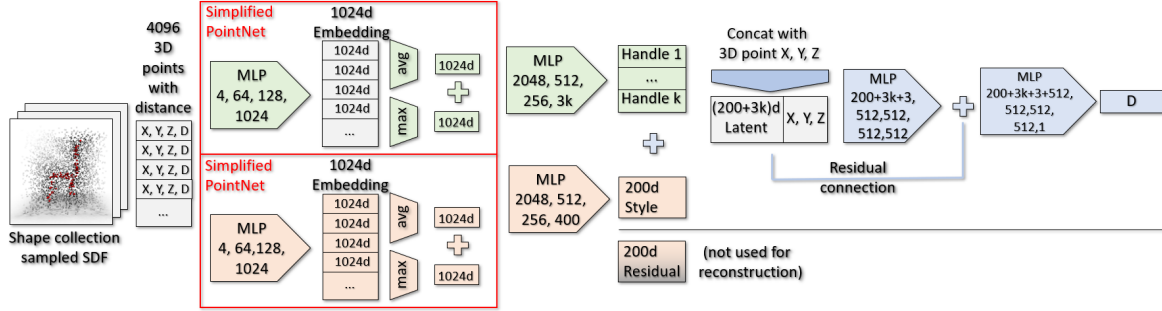


Figure 2. Our proposed architecture: Embedding and encoding an SDF through a simplified PointNet, then reconstructing the distance values through an MLP with skip connection. Note that the style- and residual encoders (orange) share an embedding for memory reasons. The handle encoder (green) is trained beforehand and then fixated.

style vector that contains any other information of the shape. The third component is the residual, which is only utilized during training to regularize the other two components and acts as a buffer to avoid inconsistent style vectors. Only the handles and the style vector make up the latent space of our autoencoder and are later used for the editing process. Then, the decoder predicts the SDF value for the given input samples from handles and style vector.

After training, we can encode a shape, move one or multiple of the handles or replace the style vector (*style transfer*), and decode the result. However, applying certain operations like moving only one side of the wings of an aircraft, are not *plausible* in the sense of the shape collection: These latent space configuration do not lie on the manifold of learned shapes that our decoder can properly decode. To find the most similar, nearest plausible shape on the manifold, we apply changes such as handle position shifts gradually throughout iterations of de- and encoding.

Difference between handles and style To train an autoencoder disentangling an input shape into style and controllable handles, we first need to define how the handles should control the output, and define style implicitly as the remaining details: Given two shapes $A(H_A)$, $B(H_B)$, with handle positions H_A , H_B , style refers to the difference between $A(H_B)$ and $B(H_B)$, *i.e.* the aspects of the shape that are not defined smoothly by handle position alone. For example, for two chairs with almost identical handle positions that only differ by a hole in the backrest, we consider this purely a stylistic difference. The definition of style is therefore directly related to the number of handle points. For an example of this, consider the car used in the top-left of Appendix D (16 handles, spoiler is expressed through handles versus 8 handles, spoiler is expressed through style).

Desired properties The latent code of our autoencoder consists of two components: the handle component (which

is supposed to control the global shape or pose of an object) and the style component (which encodes the shape differences *not* caused by handle motion). When training our network we have to make sure that the latent embedding does not degenerate. Potential threads are that the handles can encode style by micro-motions causing style changes rather than shape changes. Conversely, the style vector could encode global shape information rendering the handles useless. We prevent the former by introducing a Lipschitz-type term (Eq. (1)) into the loss function that forces changes in the latent code to be of the same magnitude as the resulting changes in the output shape and we prevent the latter by term (Eq. (2)) that penalizes changes in the style component if the shape difference can be achieved by handle motion. In addition to this, we want to keep handles and style as independent as possible which motivates another loss term (Eq. (4)).

3.1. Encoder

The encoder of our network f consists of three distinct encoders f_{eH} , f_{eS} , and f_{eR} that take a uniform random sampling of a shape SDF, S_u , as input. S_u is a set of points p with position p_{xyz} and distance p_d . All three encoders are based on a simplified PointNet [35] architecture that embeds a 4D point cloud sampled from an SDF, where the 4th dimension is the distance value to the surface. The embedding vector is then processed through a multilayer perceptron (MLP). For implementation details, see Fig. 2 and Appendix A. We require consistent handles for each shape that are either calculated from a method such as given in Sec. 3.3, or given by the user. The handle encoder $f_{eH}(S_u)$ is pre-trained to produce the given handle position. For this, the embedding vector is encoded through an MLP to form our desired handles, using a simple L2 loss. We then freeze the learned encoder part, not allowing change to the learned handles while training the rest of the network, consisting of style, residual, and decoder.

Learning the style encoder $f_{eS}(S_u)$ and the residual en-

coder $f_{eR}(S_u)$, we don't train for specific latent values, but instead add regularisation to get the desired output. To force the style vector to be used in a meaningful way and not to over-encode the information in the subtle changes of the handles, we are tethering the change in shape space to the change of latent space. We formulate a Lipschitz-like constraint per trained batch that enforces the change in the combined latent variable of style and handles to be proportional to the change in the output. We further add an individually learned weight to each handle, represented as diagonal matrix H_w . This is necessary because every region and the handle controlling it can have a different impact on the change of the SDF (e.g. consider change in the thin legs of a chair versus change in its seating area). Recall that while we learn the weights of each handle, the handle positions themselves are kept fixed. The occurring difference in the SDF of two shapes that can not be explained by the handles alone then leads to the style variable to explain all the details that differ. We thus define our loss L_{lip} regarding a batch of items B and all successive pairs of items $i, i + 1$ (to avoid a quadratically increasing number of comparisons with increasing batch sizes), where S_u^i indicates the sampling of the i th shape in the batch:

$$L_{lip} = \left(\frac{\sum_{p \in S_u^i, q \in S_u^{i+1}} |p_d - q_d| (w(p_d, S_u^i) + w(q_d, S_u^{i+1}))}{2|S_u^i|} - (||H_w f_{eH}(S_u^i) - H_w f_{eH}(S_u^{i+1})||_2 + ||f_{eS}(S_u^i) - f_{eS}(S_u^{i+1})||_2 + ||f_{eR}(S_u^i) - f_{eR}(S_u^{i+1})||_2)^2 \right) \quad (1)$$

Additionally, the sample positions are the same for all points across shapes in the batch to allow a comparison of change in the SDF value of a 3D point for two different shapes. In summary, L_{lip} penalizes the imbalance between the shape difference and the latent distance. We also use a weighting that reduces the weight of a point with distance d for a sampling S in the loss term by the distance to the surface: $w(d, S) = \max_{p_d \in S} |p_d| - |d|$. This is to take the larger importance of samples close to the surface into account. By using L_{lip} , we obtain a latent space where the change applied is proportional to the change observed in the SDF, a key attribute for the desired editability of our latent space. The individually learned weights of H_w here take the role of the Lipschitz constant reflecting the individual impact of each handle.

Keeping handles relevant To avoid disregarding handles and just encoding everything in style, we introduce an additional penalty on the style and the residual. We define:

$$L_{spen} = ||f_{eS}(S_u)||_2, \quad L_{rpen} = ||f_{eR}(S_u)||_2 \quad (2)$$

L_{lip} encourages two items with identical handles having all their differences encoded in their style vector; Opposing to that, L_{spen} encourages that for two items with very different handles, the difference in their handles is actually used in the reconstruction process as much as possible and their different looks are not just encoded in their style vectors, ignoring the handles. To capture differences between style and handle changes that can not be properly reflected in the loss and would otherwise conflict with L_{lip} , the residual part of the network is used: For two identical chairs where one of them is scaled to be wider, the resulting difference in the SDF can be explained according to L_{lip} by the change in handles. As this does not always work in a smooth and linear fashion, the resulting style vectors could be encouraged to differ. The residual absorbs these differences in a way that does not harm the generalisation of the style vector. In summary, the encoder produces a latent code consisting of style, residual, and handles that is regularized to be Lipschitz-continuous regarding change in the shape. This means having very similar input shapes produce very similar latent codes, and preferably not to encode coarse structural or pose information into the style vector. By this, we obtain a latent space disentangled into style and handle positions.

3.2. Decoder

We now describe the decoding process $f_d(f_{eH}(S), f_{eS}(S), p_{xyz})$. The latent code, consisting of the encoded style and handles, is concatenated to a 3D point p_{xyz} . We then apply a MLP to predict the distance value p_d . The latent code produced by the residual encoder $f_{eR}(S_u)$ is not used for the decoder. Now we define a reconstruction loss that measures the L2-difference between input distance and predicted signed distance for each point. To increase the quality of the learned SDF near the surface, we use another improvement inspired by Park *et al.* [34] to make the SDF sharper at the contour of the shape. We decode an additional set of surface points that are Gaussian samples S_g around the surface of the shape. This increases quality where it is most visible. Hence, we obtain a reconstruction loss that is composed of two parts (uniform and close-to-surface points) where the average weight over all samples sums up to one:

$$L_{rec} = \sum_{p \in S_u} \frac{|f_d(f_{eH}(S_u), f_{eS}(S_u), p_{xyz}) - p_d| w(p_d, S_u)}{\sum_{q \in S_u} w(q_d, S_u)} + \sum_{p \in S_g} \frac{|f_d(f_{eH}(S_u), f_{eS}(S_u), p_{xyz}) - p_d| w(p_d, S_g)}{\sum_{q \in S_u} w(q_d, S_g)} \quad (3)$$

Enforcing independence of style and handles To guarantee that our editing process works as intended, we want

the style and the handles to be independent of each other: Any combination of style and handles must still be meaningful, and an occurring change in style should not apply change to the handle positions and vice-versa. Again, as with L_{lip} , we define the loss term batch-wise by splicing each element in the batch i with the next element $i + 1$:

$$L_{ind} = ||f_{eH}(f_{d'}(f_{eH}(S_u^i), f_{eS}(S_u^{i+1}), (S_u^i)_{xyz})) - f_{eH}(S_u^i)||_2 + ||f_{eS}(f_{d'}(f_{eH}(S_u^{i+1}), f_{eS}(S_u^i), (S_u^i)_{xyz})) - f_{eS}(S_u^i)||_2 \quad (4)$$

where $f_{d'}$ means applying f_d on a set of points while $f_{d'}$ also provides xyz coordinates of each point as output to ease notation (instead of concatenating the sample xyz with the computed distance). For encoding a shape, adapting its handle (style) vector, and then de- and re-encoding the shape again should not cause any changes in the style (handles). For the complete loss function, we have the term that we train the network end-to-end with after having already trained and fixated the handle encoder f_{eH} :

$$L = \lambda_1 L_{rec} + \lambda_2 L_{lip} + \lambda_3 L_{ind} + \lambda_4 L_{rpen} + \lambda_5 L_{spen}$$

With $\lambda_1 = \lambda_2 = \lambda_3 = 100$, $\lambda_4 = 1.0$ and $\lambda_5 = 0.1$. We learn to describe an input shape through a set of handle points that must be used in the reconstruction process guided by L_{rec} . Any differences between shapes that are not encoded smoothly in the handles themselves are instead encoded in the style vector by L_{lip} . Style and handles are kept independent and exchangeable by L_{ind} , while L_{spen} prevents ignoring the handles, and L_{rpen} forces the residual to only be used if necessary. During training, $L_{lip}, L_{spen}, L_{rpen}$ are only directly regularising the encoder, while L_{rec} and L_{ind} also train the decoder.

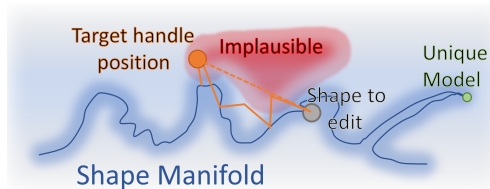
3.3. Canonical Handles

To have handles consistently at corresponding locations for shapes of a collection that we can use for editing, we need a mapping across different shapes: For intuitive editability purposes, a handle point that lies on the tip of the left wing of one airplane should be in a similar spot for another airplane. We call these consistently mapped handle points *canonical handles*. A range of approaches exist to find correspondences between shapes [9, 40, 41], but these are often slow, require well behaved geometry, or additional supervision. Instead, we use a simple procedure to find consistent correspondences between shapes of a collection. This is similar to what [28] leverage for their correspondences: To obtain a canonical set of handles that roughly correspond to the same part on every shape, we train a point cloud autoencoder called *canonicalizer*. We use PointNet as encoder and an MLP as decoder, and minimise Chamfer distance [10] between input and output. The output neurons

then localize, where the same index of the output vectors is a part of the same component throughout all shapes in the collection. These correspondences can then be used to obtain consistent, canonical handle positions throughout a shape collection. We compute a mean shape of the shape collection from the autoencoded shapes, taking the mean position for every output neuron triplet of the MLP that represents a point. We then apply farthest point sampling to obtain our handles. The exact architecture and the produced correspondences and handles can be seen in Appendix A.

3.4. Applying Adaptive Shape Editing

To perform adaptive shape editing, a given shape is encoded. Through *e.g.* a user or an automated script, the editing is performed by changing the style vector and/or the handles and decoding these again. While this process already works for some examples, the applied change does not pass on to the unedited parts: When *e.g.* making one wheel case of a car broader, it can be observed that the other wheel cases do not follow. To achieve this, we leverage a similar idea as denoising autoencoders [44], where a noised input is mapped back to the original input. Through autoencoding a gradually modified latent code of a shape, we effectively keep project back to the latent manifold of plausible shapes, as has been described by Lei *et al.* [26]. And indeed, we observe that for slightly noised latent codes of examples from our shape collection in the latent code, de- and encoding them again moves them closer to the original latent code, hence back to the manifold of plausible shapes.



We further observe that very unique items form their

own sub-part of the manifold, offering fewer plausible latent directions for editing (see Appendix C for a deeper analysis).

Editing in latent space and keeping shapes meaningful

In practise, only regions of the latent space close to the shape manifold are properly regularized. If we move too far from the manifold, iterating the decoding and encoding process will not move us back to a plausible shape. To avoid this, we apply all edits to the shape through multiple rounds. We gradually apply change to the latent code by moving a handle at most by 0.075 units towards the target direction for a shape collection normalized to the unit cube. This ensures we do not leave the manifold without being able to project back to it. For all shape edits in this paper, we used at most 10 rounds and ended earlier if we had the handle move less than 0.03 units close to its target

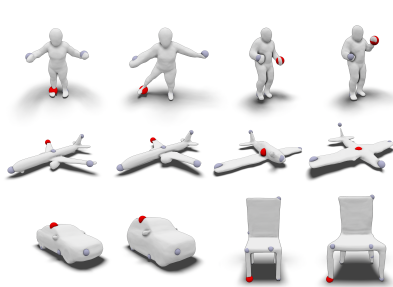


Figure 3. Examples of editing shapes moving the handles (red, always pairs of before- and after editing).

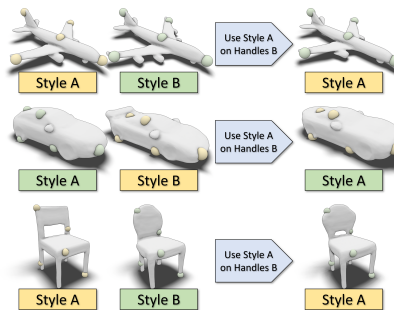


Figure 4. Examples of editing shapes by transferring style through exchanging style vectors.

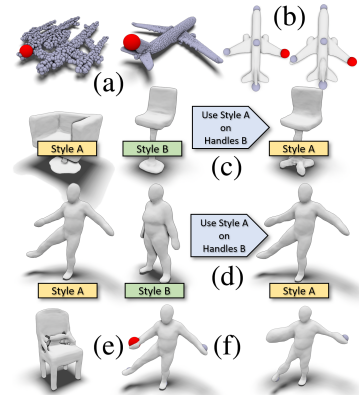


Figure 5. Examples of failure cases.

in an iteration. This is to prevent iterations where we keep projecting back to the manifold from an implausible configuration, *e.g.* when moving a chair leg beneath the ground plane. For an example of different editing operations using handles, see Fig. 3. We also keep the style vector fixed for handle editing. To transfer the style from one shape to another, we simply encode two shapes, swap out their style vector, and decode them. For an example of different style transfer examples, see Fig. 4.

4. Evaluation

To evaluate our framework, we picked shape collections with varying characteristics. For our chosen man-made shapes (airplanes, tables, cars, chairs from Shapenet [5]) and organic shapes (FAUST [4]), diverse properties have to be implicitly learned. These can include learning symmetry, physical properties like no freely floating parts, and plausible poses of bodies. For the qualitative analysis, we show a broad selection of editing results through handle- or style manipulation and aim to explain the failure cases that have occurred. While providing quantitative results for a shape editing framework is somewhat ill-posed, we instead provide quantitative analysis of the key properties that a shape editing tool should have: Expressiveness and the learned underlying semantics that are used in the editing process. For expressiveness and quality, we utilize the same metric as [30], showing that our framework is similarly powerful as the state of the art. Regarding semantics, we compare ourselves to semantic segmentation approaches, using an ad hoc way of extracting a segmentation from our learned network.

4.1. Qualitative Analysis

We observe a large shape space that can produce many plausible variations that do not exist in the original shape collection, see Fig. 8. For a larger collection of results,

see Appendix D. Using the technique described in Sec. 3.3, we find that the produced handles are of mostly sufficient quality for man-made objects. However, for deformed, non-trivial shapes such as human poses from the FAUST Dataset or atypical shapes, the handles show inconsistencies. Consequently, we hand-pick handles using the given correspondences for the FAUST Dataset. For all other items we use the canonicalization technique described.

Disentanglement into style and handles The decomposition of an input shape into handles and style is strongly dependent on the number of handles used. Where *e.g.* for a large number of handles on an airplane, the engines will have a handle controlling them instead of being encoded in the style. Style transfer is also highly dependent on the setting it is used in and may not produce any useful characteristics. For chairs, the style is only meaningfully transferable for some examples (see Fig. 5c). For FAUST, style encodes mostly the body type, but breaks down for very unique poses like a flying kick (see Fig. 5d). Examples of style transfer can be seen in Fig. 4.

Shape collection biases We observe shape collection given biases, *e.g.* when changing the handle position of an airplane to be more bent backwards into delta wings, the engines will start to shrink and a rear engine can start to form (see Fig. 5b). While this seems like bad generalisation, a closer look at the shape collection shows that most airplanes with delta wings are having their engines tightly integrated into their wings, and airplanes with wings bent more backwards often have a rear engine. Hence, there is a plausible shift in the optics in what might be perceived as change in style.

Limitations While editing works well on most examples and style transfer has meaningful cases, we also observe

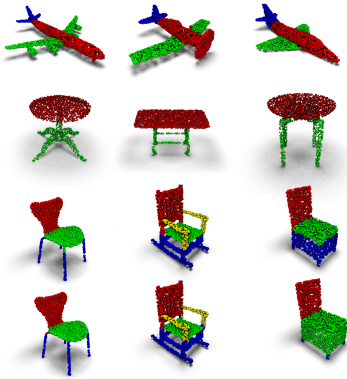


Figure 6. Segmentations, with the last row showing the ground truth for chairs.

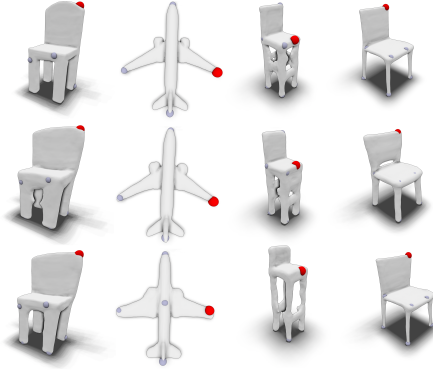


Figure 7. Ablation. Top to bottom: Input, ablated, complete. Left to right: No residual, no independence loss, no style penalty, no Lipschitz penalty.

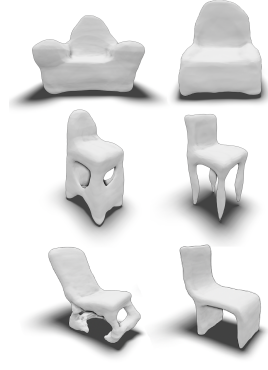


Figure 8. Generated shapes (left) and the closest item from the shape collection.

a number of failure modes. For large shape collections like Shapenet that *e.g.* contain a star destroyer in the plane dataset, lack of quality and specificity can be expected for a net with only 4 million parameters. However, we observe that even the badly reconstructed items (*e.g.* Fig. 5e) follow some semantics, like remaining symmetric. Editing very unique shapes will at times not work at all (see Fig. 5f). We can partly explain this as these shapes forming (partially) their own separated component of the shape manifold, leading to any small change to be snapped right back through re-encoding. For a detailed analysis, see Appendix C. This can be seen as an indication of a well-trained latent space: A single example should not be generalized upon. However, this does mean that some shapes are not editable at all. We also observe that style transfer is the most meaningful for shapes where the handles are in similar positions. For example, bar stools with a very unique handle position will barely gain any predictable/meaningful characteristics from using the style of sofas. Lastly, the quality of the input handles can vary greatly and they can be placed poorly or inconsistent through the artifacts that a pointcloud-based autoencoder causes, see Fig. 5a. Additionally, Shapenet in general comes in incredible variety, and generalisation is more difficult when there are *e.g.* chairs with separate footrests, rows of chairs, and quirky designer items in the collection. While these issues are not ideal, most of them can be plausibly explained and fixed in the future by a more complex network (quality), careful dataset curation and augmentation (bridging the gap to isolated items, throwing out shapes that hinder generalisation), and better handles (style disentanglement not working properly and difficulties editing).

Structured analysis The reconstruction quality L_{rec} together with the pre-trained handle encoder alone might already lead to good results. To show that this is not the case and our loss is not unnecessarily complex, we provide

Method	Chair		Car		Table	
	COV \uparrow	MMD \downarrow	COV \uparrow	MMD \downarrow	COV \uparrow	MMD \downarrow
3DN [46]	32.0	4.56	46.6	2.91	30.6	4.26
CC [15]	51.0	4.26	50.3	2.79	50.2	3.88
NC [49]	54.4	4.23	66.6	2.65	44.7	3.85
DMH [30]	64.6	4.28	76.5	2.97	54.9	3.70
Ours	52.3	4.20	60.1	2.53	44.0	3.99

Table 1. Results of computing COV and MMD on Shapenet Classes, COV in percent, MMD in Chamfer distance times 100. High COV and low MMD is desired. Other numbers taken from the work of Liu *et al.* [30].

the following ablation (see Fig. 7 for illustrations): When not using a residual, a handle change may force unwanted change in the output to satisfy the proportionality of change in latent space versus change in output (L_{lip}). This can be absorbed by the residual. Without L_{ind} , editing may fail because the net only plausibly decodes certain combinations of style and handles, and the manifold re-projection then just maps back to the original input. Using no style penalty, L_{lip} can be circumvented by *e.g.* encoding everything in the style vector. In result, changes in handles can lead to no change in the output. Lastly, without L_{lip} , we may get rather large changes in shape from small latent changes, *e.g.* small handle shifts causing genus changes. While sometimes our approach works without one of the loss components, we observe a significant increase in quality of the editing process when using all proposed losses.

4.2. Quantitative Analysis

Generative properties Liu *et al.* [30] judge the resulting quality of their learned deformation space by splitting the shape collection in two groups A (500 items) and B (remaining items), where each item in A is used to generate

Method	Airplane(3)	Chair(4)	Table(2)
PointNet† [35]	70.6	83.7	72.5
PointNet++† [36]	72.2	86.1	74.1
PointCNN† [29]	71.7	83.4	62.5
BAE-Net [7]	61.1	83.7*	78.7
Ours	67.5	65.7	73.8

Table 2. Segmentation accuracy in percent for (k) segments. † indicates a supervised approach using 5 percent of the data for labels, others are unsupervised. Numbers for the previous approaches taken from the work of Chen *et al.* [7].

20 variations, and B is used to evaluate the quality of these variations. *Coverage* (COV) describes how many different shapes from B are the closest shape for any variation of A under Chamfer distance, and *minimum matching distance* (MMD) [1] describes the minimum Chamfer distance of each item in B to the closest item from the variations of A . To generate a plausible variation, we gradually move one random handle towards the handle position from another random sample from A , using 4 iterations while not holding the style vector fixated. The outputs are then extracted by marching cubes and sampled with 4096 points¹, normalized to a unit sphere, and leveled to the ground plane. While we can not reach [30] in all quantitative results, we show that our approach is still versatile. Usability, which is the main focus of our work, is not measurable through MMD and coverage, it is generally hard to quantify. For the (partially) better MMD values, we argue that the 3-dimensional degree of change we can apply to a handle can better fit certain shapes, as Liu *et al.* can only apply 1-dimensional change on a metahandle.

Segmentation We observed a close relationship between learned handles and semantic meaningful regions of the encoded shape. To use this relationship for unsupervised part segmentation, we propose an ad hoc method. We apply a large number of small deformations through individual handles and measure the SDFs behavior at sampled surface points. These changes in the SDF then form feature vectors that are used to measure how different sample points are correlated, building a knn graph on the neighborhoods of points. On this graph, spectral clustering then yields a segmentation of the surface samples into a desired number of parts. Technical details can be found in Appendix B.

¹Liu *et al.* use 100000 samples, resulting in computing $500 \times 20 \times |B|$ Chamfer distance values with a distance matrix each of 100000^2 entries. To save resources, we only used 4096 points. We observe that simply scaling the Chamfer distance with a coefficient computed on the shape collection yields the correct Chamfer distance within 1/2/4 percent error (table/chair/car) of the distance value computed with 100000 samples. A derivation of Chamfer distance that takes the mean of euclidean distances instead is used.

For a comparison of our unsupervised segmentation results, we use the shape collection and scores provided by BAE-Net [7], see Tab. 2. We compare in particular to BAE-Net, as it is also an unsupervised approach utilizing SDFs. They segment their input by having an autoencoder with multiple decoders, each one specializing on different segments of the shape collection.

Despite our approach solely operating on changes in the SDF, we obtain semantically reasonable decompositions that are (in part) comparable to the state of the art. Examples can be seen in Fig. 6, which also shows a failure mode: As the ground truth is annotated by humans, we can obtain a segmentation that is technically different, yet could be considered plausible. Also note that the result of Chen *et al.* on chairs is only possible as they join classes of chairs and tables during training. As our method was only a simple demonstration of the semantics embedded in the handles and not the focus of our work, we did not perform such optimizations and expect further improvements to be possible. We conclude that the active regions of individual handles are strongly related to high-level characteristics of the underlying shape domain.

5. Conclusion

We introduce an autoencoder that learns to encode a manipulable latent representation from an input shape. Through tethering change in the latent space to change in the shape space, we decompose our latent representation into style and handles. By passing manipulated latent codes through our autoencoder multiple times, we obtain a degree of plausibility within the range of the learned shape collection. While the quality of the produced outputs is generally satisfying, we think that improvement through more powerful encoder and decoder architectures, more carefully chosen or augmented shape collections, and more consistent handle positions is possible. We see possibilities to extend beyond the domain of geometry, *e.g.* learning to manipulate photos of people by using facial landmarks as handles. Learning handles end-to-end instead of in a separate step could also increase performance and learned semantics. The results generated from our framework show that the network learned underlying semantics that can be used for various tasks. This was demonstrated by performing various editing operations on a qualitative, and segmentation and model generation on a quantitative level. We expect many more applications, *e.g.* symmetry detection, to be possible.

References

- [1] Panos Achlioptas, Olga Diamanti, Ioannis Mitliagkas, and Leonidas Guibas. Learning representations and generative models for 3d point clouds. In *International conference on machine learning*, pages 40–49. PMLR, 2018. 8

- [2] Matan Atzmon, David Novotny, Andrea Vedaldi, and Yaron Lipman. Augmenting implicit neural shape representations with explicit deformation fields. *arXiv preprint arXiv:2108.08931*, 2021. 2
- [3] Tristan Aumentado-Armstrong, Stavros Tsogkas, Allan Jepson, and Sven Dickinson. Geometric disentanglement for generative latent shape models. In *Proceedings of the IEEE/CVF International Conference on Computer Vision*, pages 8181–8190, 2019. 2
- [4] Federica Bogo, Javier Romero, Matthew Loper, and Michael J Black. Faust: Dataset and evaluation for 3d mesh registration. In *Proceedings of the IEEE Conference on Computer Vision and Pattern Recognition*, pages 3794–3801, 2014. 6
- [5] Angel X Chang, Thomas Funkhouser, Leonidas Guibas, Pat Hanrahan, Qixing Huang, Zimo Li, Silvio Savarese, Manolis Savva, Shuran Song, Hao Su, et al. Shapenet: An information-rich 3d model repository. *arXiv preprint arXiv:1512.03012*, 2015. 6
- [6] Xi Chen, Yan Duan, Rein Houthoofd, John Schulman, Ilya Sutskever, and Pieter Abbeel. Infogan: Interpretable representation learning by information maximizing generative adversarial nets. *CoRR*, abs/1606.03657, 2016. 1
- [7] Zhiqin Chen, Kangxue Yin, Matthew Fisher, Siddhartha Chaudhuri, and Hao Zhang. Bae-net: branched autoencoder for shape co-segmentation. In *Proceedings of the IEEE/CVF International Conference on Computer Vision*, pages 8490–8499, 2019. 8, 11
- [8] Ellen Dekkers, Leif Kobbelt, Richard Pawlicki, and Randall C Smith. A sketching interface for feature curve recovery of free-form surfaces. In *2009 SIAM/ACM Joint Conference on Geometric and Physical Modeling*, pages 235–245, 2009. 1
- [9] Danielle Ezuz, Justin Solomon, and Mirela Ben-Chen. Reversible harmonic maps between discrete surfaces. *ACM Transactions on Graphics (TOG)*, 38(2):1–12, 2019. 5
- [10] Haoqiang Fan, Hao Su, and Leonidas J Guibas. A point set generation network for 3d object reconstruction from a single image. In *Proceedings of the IEEE conference on computer vision and pattern recognition*, pages 605–613, 2017. 5
- [11] Yutong Feng, Yifan Feng, Haoxuan You, Xibin Zhao, and Yue Gao. Meshnet: Mesh neural network for 3d shape representation. In *Proceedings of the AAAI Conference on Artificial Intelligence*, volume 33, pages 8279–8286, 2019. 2
- [12] Matheus Gadelha, Giorgio Gori, Duygu Ceylan, Radomir Mech, Nathan Carr, Tamy Boubekeur, Rui Wang, and Subhransu Maji. Learning generative models of shape handles. In *Proceedings of the IEEE/CVF Conference on Computer Vision and Pattern Recognition*, pages 402–411, 2020. 2
- [13] Lin Gao, Jie Yang, Tong Wu, Yu-Jie Yuan, Hongbo Fu, Yu-Kun Lai, and Hao Zhang. Sdm-net: Deep generative network for structured deformable mesh. *ACM Transactions on Graphics (TOG)*, 38(6):1–15, 2019. 2
- [14] Ian Goodfellow, Jean Pouget-Abadie, Mehdi Mirza, Bing Xu, David Warde-Farley, Sherjil Ozair, Aaron Courville, and Yoshua Bengio. Generative adversarial nets. *Advances in neural information processing systems*, 27, 2014. 1
- [15] Thibault Groueix, Matthew Fisher, Vladimir G Kim, Bryan C Russell, and Mathieu Aubry. Unsupervised cycle-consistent deformation for shape matching. In *Computer Graphics Forum*, volume 38, pages 123–133. Wiley Online Library, 2019. 7
- [16] Michael Hagenlocker and Kikuo Fujimura. Cffd: a tool for designing flexible shapes. *The Visual Computer*, 5(14):271–287, 1998. 1
- [17] Rana Hanocka, Noa Fish, Zhenhua Wang, Raja Giryes, Shachar Fleishman, and Daniel Cohen-Or. Alignet: partial-shape agnostic alignment via unsupervised learning. *ACM Transactions on Graphics (TOG)*, 38(1):1–14, 2018. 2
- [18] Kenneth P Herndon, Andries Van Dam, and Michael Gleicher. The challenges of 3d interaction: a chi’94 workshop. *ACM SIGCHI Bulletin*, 26(4):36–43, 1994. 1
- [19] Irina Higgins, Loic Matthey, Arka Pal, Christopher Burgess, Xavier Glorot, Matthew Botvinick, Shakir Mohamed, and Alexander Lerchner. beta-vae: Learning basic visual concepts with a constrained variational framework. 2016. 1, 2
- [20] Tero Karras, Samuli Laine, and Timo Aila. A style-based generator architecture for generative adversarial networks. In *Proceedings of the IEEE/CVF Conference on Computer Vision and Pattern Recognition*, pages 4401–4410, 2019. 1
- [21] Tero Karras, Samuli Laine, Miika Aittala, Janne Hellsten, Jaakko Lehtinen, and Timo Aila. Analyzing and improving the image quality of stylegan. In *Proceedings of the IEEE/CVF Conference on Computer Vision and Pattern Recognition*, pages 8110–8119, 2020. 1
- [22] Diederik P Kingma and Jimmy Ba. Adam: A method for stochastic optimization. *arXiv preprint arXiv:1412.6980*, 2014. 11
- [23] Diederik P Kingma and Max Welling. Auto-encoding variational bayes. *arXiv preprint arXiv:1312.6114*, 2013. 1
- [24] M. Kleineberg. Mesh to sdf. https://github.com/marian42/mesh_to_sdf, 2020. 11
- [25] Mark A Kramer. Nonlinear principal component analysis using autoassociative neural networks. *AICHE journal*, 37(2):233–243, 1991. 1
- [26] Na Lei, Dongsheng An, Yang Guo, Kehua Su, Shixia Liu, Zhongxuan Luo, Shing-Tung Yau, and Xianfeng Gu. A geometric understanding of deep learning. *Engineering*, 6(3):361–374, 2020. 5
- [27] Chun-Liang Li, Manzil Zaheer, Yang Zhang, Barnabas Poczos, and Ruslan Salakhutdinov. Point cloud gan. *arXiv preprint arXiv:1810.05795*, 2018. 1
- [28] Ruihui Li, Xianzhi Li, Ka-Hei Hui, and Chi-Wing Fu. Sp-gan: sphere-guided 3d shape generation and manipulation. *ACM Transactions on Graphics (TOG)*, 40(4):1–12, 2021. 5
- [29] Yangyan Li, Rui Bu, Mingchao Sun, Wei Wu, Xinhan Di, and Baoquan Chen. Pointcnn: Convolution on x-transformed points. *Advances in neural information processing systems*, 31:820–830, 2018. 8
- [30] Minghua Liu, Minhyuk Sung, Radomir Mech, and Hao Su. Deepmetahandles: Learning deformation meta-handles of 3d meshes with biharmonic coordinates. In *Proceedings of the IEEE/CVF Conference on Computer Vision and Pattern Recognition*, pages 12–21, 2021. 1, 2, 6, 7, 8

- [31] Ilya Loshchilov and Frank Hutter. Fixing weight decay regularization in adam. *CoRR*, abs/1711.05101, 2017. [11](#)
- [32] Mehdi Mirza and Simon Osindero. Conditional generative adversarial nets. *CoRR*, abs/1411.1784, 2014. [1](#)
- [33] Kaichun Mo, Paul Guerrero, Li Yi, Hao Su, Peter Wonka, Niloy Mitra, and Leonidas J Guibas. Structurenet: Hierarchical graph networks for 3d shape generation. *arXiv preprint arXiv:1908.00575*, 2019. [2](#)
- [34] Jeong Joon Park, Peter Florence, Julian Straub, Richard Newcombe, and Steven Lovegrove. Deepsdf: Learning continuous signed distance functions for shape representation. In *Proceedings of the IEEE/CVF Conference on Computer Vision and Pattern Recognition*, pages 165–174, 2019. [2](#), [4](#), [11](#)
- [35] Charles R Qi, Hao Su, Kaichun Mo, and Leonidas J Guibas. Pointnet: Deep learning on point sets for 3d classification and segmentation. In *Proceedings of the IEEE conference on computer vision and pattern recognition*, pages 652–660, 2017. [3](#), [8](#)
- [36] Charles R Qi, Li Yi, Hao Su, and Leonidas J Guibas. Pointnet++: Deep hierarchical feature learning on point sets in a metric space. *arXiv preprint arXiv:1706.02413*, 2017. [8](#)
- [37] Ali Razavi, Aaron van den Oord, and Oriol Vinyals. Generating diverse high-fidelity images with vq-vae-2. In *Advances in neural information processing systems*, pages 14866–14876, 2019. [1](#)
- [38] Sashank J Reddi, Satyen Kale, and Sanjiv Kumar. On the convergence of adam and beyond. *arXiv preprint arXiv:1904.09237*, 2019. [11](#)
- [39] Emanuel Sachs, Andrew Roberts, and David Stoops. 3-draw: A tool for designing 3d shapes. *IEEE Computer Graphics and Applications*, 11(06):18–26, 1991. [1](#)
- [40] Patrick Schmidt, Marcel Campen, Janis Born, and Leif Kobbelt. Inter-surface maps via constant-curvature metrics. *ACM Transactions on Graphics (TOG)*, 39(4):119–1, 2020. [5](#)
- [41] John Schreiner, Arul Asirvatham, Emil Praun, and Hugues Hoppe. Inter-surface mapping. In *ACM SIGGRAPH 2004 Papers*, pages 870–877. 2004. [5](#)
- [42] Minhyuk Sung, Zhenyu Jiang, Panos Achlioptas, Niloy J Mitra, and Leonidas J Guibas. Deformsyncnet: Deformation transfer via synchronized shape deformation spaces. *arXiv preprint arXiv:2009.01456*, 2020. [2](#)
- [43] Qingyang Tan, Lin Gao, Yu-Kun Lai, and Shihong Xia. Variational autoencoders for deforming 3d mesh models. In *Proceedings of the IEEE conference on computer vision and pattern recognition*, pages 5841–5850, 2018. [2](#)
- [44] Pascal Vincent, Hugo Larochelle, Yoshua Bengio, and Pierre-Antoine Manzagol. Extracting and composing robust features with denoising autoencoders. In *Proceedings of the 25th international conference on Machine learning*, pages 1096–1103, 2008. [5](#)
- [45] Nanyang Wang, Yinda Zhang, Zhuwen Li, Yanwei Fu, Wei Liu, and Yu-Gang Jiang. Pixel2mesh: Generating 3d mesh models from single rgb images. In *Proceedings of the European Conference on Computer Vision (ECCV)*, September 2018. [2](#)
- [46] Weiyue Wang, Duygu Ceylan, Radomir Mech, and Ulrich Neumann. 3dn: 3d deformation network. In *Proceedings of the IEEE/CVF Conference on Computer Vision and Pattern Recognition*, pages 1038–1046, 2019. [7](#)
- [47] Wen Xiao, Zhenan Fan, and Qiuyan Liu. Point cloud generation via variational auto-encoder. [2](#)
- [48] Jie Yang, Kaichun Mo, Yu-Kun Lai, Leonidas J Guibas, and Lin Gao. Dsm-net: Disentangled structured mesh net for controllable generation of fine geometry. *arXiv preprint arXiv:2008.05440*, 2020. [2](#)
- [49] Wang Yifan, Noam Aigerman, Vladimir G Kim, Siddhartha Chaudhuri, and Olga Sorkine-Hornung. Neural cages for detail-preserving 3d deformations. In *Proceedings of the IEEE/CVF Conference on Computer Vision and Pattern Recognition*, pages 75–83, 2020. [2](#), [7](#)
- [50] M Ersin Yumer and Niloy J Mitra. Learning semantic deformation flows with 3d convolutional networks. In *European Conference on Computer Vision*, pages 294–311. Springer, 2016. [2](#)
- [51] Xiaohu Zhang, Yuexian Zou, and Wei Shi. Dilated convolution neural network with leakyrelu for environmental sound classification. In *2017 22nd International Conference on Digital Signal Processing (DSP)*, pages 1–5. IEEE, 2017. [11](#)

Appendices

A. Implementation Details

In this section, we give detailed information on how the samples are prepared, on the fine details of the architecture, on how our network is trained, and on how the output images seen throughout this work are extracted. We use the approach of Kleineberg [24] to sample our shape collections, as the Shapenet datasets are *e.g.* not watertight. All shapes are centered and placed on the ground plane at $z = -1$ / airplanes at $z = -0.5$ while making sure the largest dimension of their bounding box is 2 units wide, while taking SDF samples uniform randomly in the range of $[-1.1, 1.1]$ for each coordinate axis.

Architecture For the embedding, we use 1d convolution with kernel size 1 to increase from 3 (canonicalizer)/4 (main network) to (64, 128, 1024) channels per point, then applying both max pooling and average pooling to obtain two 1024 dimensional embedding vectors that we concatenate. For the canonicalizer, this is then encoded to a 256-dimensional embedding vector through three linear layers (512, 256, 256), and then reconstructed to a full point cloud of 2048 3D points through 3 final linear layers (256, 512, 6144). The architecture and output can be seen in Fig. 9, a visualisation of the consistency can be found in Fig. 10. Note that the consistency is becoming weaker for unique shapes, see the rear of the bottom-right example. For the main network, we apply two separate encoders (one for handles, one joint for style and residual) on the embedding vector, reducing the number of channels to 512, then 256, then the desired target size. For all experiments in this paper, we used a 200 dimensional latent vector for style and residual each, while using 3 neurons per handle point. For the decoder, we combine handles and style vector into a single latent vector, concatenate the desired point to decode, and then apply an MLP for 8 layers with channel size 512 and a residual connection from the latent vector to the 5th layer of the MLP. Note that this is the same decoder architecture as DeepSDF [34]. In total, our network had 4.5 million parameters. For all layers, except the actual output layers and the layers that produce style, residual, and handles, we used a LeakyReLU [51] as non-linearity.

Training and mesh extraction All networks are trained using the ADAM-W optimizer [22,31] with AMSGrad [38], weight decay rate of 0.005 on the main network, batch size 16, no weight decay on the canonicalizer, learning rate 0.001, tuned down to 0.0002 after 500 epochs, and otherwise default parameters. We found that the networks were fairly robust regarding adaptations of the parameters and the

varying domains of the shape collections used. No form of normalisation was used. All examples seen in this paper have been trained for 3 days on a single GeForce RTX 2080 Ti, resulting in between 1000 and 2300 epochs, depending on the shape collection. Training for longer periods of time did not show any significant improvements.

We extract all examples in this work by using marching cubes at a resolution of 200 with a level of 0 to 0.05, depending on how filigree the output is. For example, thin parts like airplane wings rarely have a sample directly inside them. This results in the SDF at times never reaching to zero (or below). Using a level slightly larger than zero then yields a less fringed output.

B. Shape Segmentation Procedure

To segment a given 3D mesh, we first need a distinct set of points where to measure the change of the SDF. In our comparison, we used the pre-computed sample points provided by Chen *et al.* [7] to better compare our results. Additionally, we sample the shapes SDF to compute the handle and style vector. Next we separately apply a Gaussian 3D shift to each handle and measure the resulting absolute change in the SDF value of each surface sample. To keep the shift magnitude in a reasonable range for each shape, at each segmentation we compute the standard deviation of all surface samples along the three axes and scale the shift by the minimum axis deviation value. Repeating the random shifts and distance measurements 1024 times yields a $h \times 1024$ feature descriptor per sample, where h is the number of handles. Averaging this descriptor over the different shifts indicates the response of a samples distance value to a moving handle (see Fig. 11). As some handles generally affect distance values more than others, but similar feature magnitudes are desired, all descriptor values originating from the same handle are divided by their joint $l1$ -norm. To remove the large difference between highly active and almost inactive surface samples regarding distance changes, all values originating from the same sample are also divided by their joint $l1$ -norm. To obtain segmented parts, we build a knn-graph in the feature descriptor space with neighborhoods spanning over 5 percent of the total number of surface samples. Each edge between neighboring samples i and j is given a similarity weight $s_{i,j}$ formulated as:

$$s_{i,j} = e^{-\frac{\|f_i - f_j\|}{\|f_i\| \cdot \|f_j\|}} \quad (5)$$

where f_i and f_j are the flattened feature descriptors of both samples. Applying spectral clustering now yields an assignment for each of the points to one of the labels, which we in turn then can map back from the individual points to the input mesh. In contrast to BAE-Net we do need to specify the exact number of expected parts instead of an upper limit for the chairs shape collection where some segments

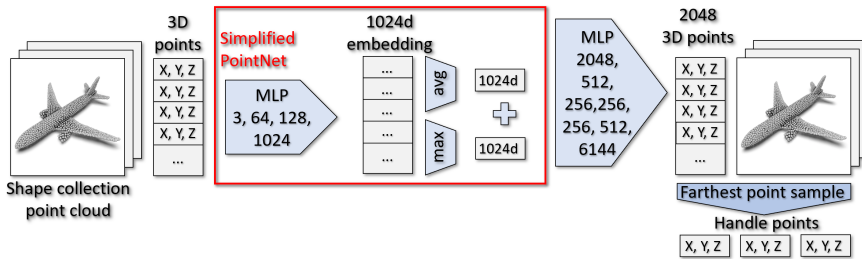


Figure 9. The simple architecture used to obtain correspondences between different shapes in a collection. The neurons of each output point specialize, with each point always being in a similar semantic part of the shape.

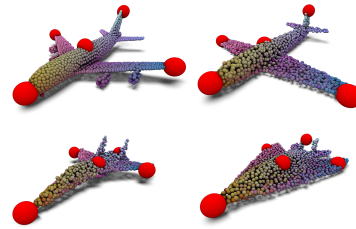


Figure 10. The RGB coloring is computed on the top-left input per axis, mapping the relative X/Y/Z positions to RGB colors. Consistent colors then used across shapes.



Figure 11. Response to 1024 random changes in one handle at the wing tip, here averaged. Brighter means more response.

do not always occur (e.g. not all chairs have armrests). As spectral clustering does not output consistent indices for the part classes, we further apply a mapping to the ground truth indexing in the score calculation.

C. Exploration of the Manifold

To explore the properties of the latent manifold produced by our autoencoder, we provide two additional experiments on the chairs dataset:

Reprojection We show that our autoencoder has similar properties to a noisy autoencoder, *i.e.* decoding and encoding a noised shape (*i.e.* noised latent code) reduces the amount of noise. For this, we apply a random shift in $[-0.03, 0.03]$ to dimension of the latent code, then en- and decode and measure the absolute mean difference between the original and the re-projected latent code. We then compare this to the random change in latent we initially applied. For 1000 such operations on a random chair, we only have an average of 59.5 percent and a median of 56.2 percent of the noise remaining after a single re-projection. Note that some part of the remaining difference can also be explained by shifts in the latent that are actually moving along the manifold of plausible shapes. This shows properties similar to a noisy autoencoder, enabling us to re-project back to a

plausible shape through encoding and decoding steps.

Unique shapes are bad for editing We show that shapes that are irregular are indeed worse for editing, *i.e.* forming their own distinct region on the manifold of plausible shapes. While this does not hold for every special shape, we can observe a general tendency towards snapping back to the old latent handle positions / latent in general when performing editing operations. This indicates a low editability. We demonstrate this by taking the 100 examples from our shape collection where the handles are least/most unique, measured in distance to the next most similar handle constellation in euclidean distance. We then apply 10 random deformations on each of the handle latent codes by applying a random shift in $[-0.1, 0.1]$, then de- and encode again. We measure that the unique chairs lose 76/75 (average/median) percent of the edit applied through re-encoding, whereas the least unique chairs only lose 58/58 (average/median) percent of the edit. Hence, a very unique chair is much less editable, having fewer plausible deformation directions in the latent space. Conversely, a non-unique chair re-trains much more of the change applied after being re-projected to the manifold of plausible shapes. Note that uniqueness from handle position alone does not reflect on the uniqueness of their style vector, *i.e.* their uniqueness in general, and is only a crude experiment. However, this still backs our observation: More extreme and unique shapes are less editable and are re-projected more to their original latent code when being edited, retaining much less of an edit process, as the common chair types generalise better.

D. More results

We show more results from our editing procedure in Fig. 12. Note how the car on the top-left is using 16 handles, showing the spoiler being part of the handle configuration. Using 8 handles, the spoiler instead becomes part of the style, as can be seen below.



Figure 12. More selected results from the editing process.